can be obtained, and the chemical products produced by photolysis appear already separated in isolated cell compartments.

(4) In a comparison with semiconductor PEC cells there are a number of advantages. There are no complications or requirements arising from photolysis at an interface or from materials problems such as electrode photodecomposition. The electrode acts only as a "collector". The quantitative details of the cells are determined by homogeneous photochemical reactions, which can be studied with use of routine experimental techniques (e.g., luminescence quenching, quantum yield determination, and flash photolysis), and their current/voltage/time characteristics are derivable in a straightforward fashion.[9] It follows that the maximization of cell performance is a chemical problem solvable by synthesis and measurements in solution rather than a problem in solid-state physics.

(5) Specifically, when the problem of water splitting or other solar to chemical energy conversion schemes is dealt with, the cells may find direct application. Following either oxidative or reductive quenching, water must enter the scheme, probably in a catalyzed step, as either an oxidative or a reductive "scavenger". One example of a workable scheme based on $Ru(bpy)_3^{2+}$ is shown in Scheme III. It relies on initial oxidative quenching followed by the reduction of water by the reduced quencher. The reduction of water must be made to occur on a time scale that is short compared to back electron transfer between $Ru(bpy)_3^{3+}$ and red. The energy conversion cycle could be completed on a relatively leisurely time scale by electrochemical oxidation of H_2O by $Ru(bpy)_3^{3+}$ in a separate cell compartment. Given the relatively low intensity of the solar flux, the demands placed on electrodes in terms of current densities are far less than those associated with fuel cells.

Scheme III

$$Ru(bpy)_3^{2+} \xrightarrow{h\nu} Ru(bpy)_3^{2+*}$$

$$Ru(bpy)_3^{2+*} + ox \rightarrow Ru(bpy)_3^{3+} + red$$

$$red + H_2O \rightarrow ox + {}^1/_2H_2 + OH^-$$

$$Ru(bpy)_3^{3+} + e^- \xrightarrow{Pt} Ru(bpy)_3^{2+}$$

$$OH^- \xrightarrow{Pt} {}^1/_4O_2 + {}^1/_2H_2O + e^-$$

(6) The possibilities for developing other energy storage reactions based on excited-state PEC cells are clear.[26-29] It should be reemphasized that one of the real values of such cells is their basis in homogeneous photochemistry since further developments in that area will provide the basis for additional cells. The experimental bases for individual half-cells can be studied separately and combined later in a net cell.

Acknowledgments are made to the National Science Foundation for a fellowship for W.J.D., to the Chaim Weizmann Postdoctoral Fellowship Program for fellowship support for B.D., and to the Department of Energy under Grant No. DE-A505-78ER06034 for support of this research.

Registry No. H_2, 1333-74-0; O_2, 7782-44-7; $Ru(bpy)_3^{2+}$, 15158-62-0.

(28) Chandrasekaran, K.; Whitten, D. G. *J. Am. Chem. Soc.* **1980**, *102*, 5119.

(29) Sullivan, B. P.; Dressick, W. J.; Meyer, T. J. *J. Phys. Chem.* **1982**, *86*, 1473.

Contribution from Department of Chemistry, Texas A&M University, College Station, Texas 77843

Electronic Structure of Metal Clusters. 2. Photoelectron Spectrum and Molecular Orbital Calculations of Decacarbonyldihydridotriosmium

DAVID E. SHERWOOD, JR., and MICHAEL B. HALL*

Received December 3, 1981

Molecular orbital (MO) calculations and the gas-phase ultraviolet photoelectron (PE) spectrum are reported for $H_2Os_3(CO)_{10}$. In a comparsion with the PE spectrum of $Os_3(CO)_{12}$, the major spectral change is loss of a band due to a direct Os–Os bond and appearance of bands due to Os–H–Os bridge bonds. The spectrum also shows a substantial rearrangement of the bands due to the pseudo-t_{2g} electrons, which are usually considered Os–CO π bonding but Os–Os nonbonding. The molecular orbital results, which are described in terms of the pseudooctahedral fragments, $Os(CO)_4$ and $Os(CO)_3$, suggest that the rearrangement of the pseudo-t_{2g} electrons results in a partial Os–Os bond between the hydrogen-bridged osmiums. The calculations also suggest that donation into a low-lying Os–Os antibonding orbital is responsible for the increase in Os–Os bond distance as bridging hydrogens are replaced by bridging methoxide groups.

Introduction

There has been a great deal of interest in the chemistry, structure, and bonding of decacarbonylbis(μ-hydrido)-*triangulo*-triosmium, $(\mu\text{-}H)_2Os_3(CO)_{10}$, since it was first synthesized by Johnson, Lewis, and Kilty.[1] This complex undergoes oxidative addition with alkenes[2] and alkynes,[3] under much milder reaction conditions than the simple parent carbonyl species, dodecacarbonyl-*triangulo*-triosmium, $Os_3(CO)_{12}$. Two-electron-donor ligands, L (L = carbonyl, phenyl cyanide, or phosphines), can add associatively to $(\mu\text{-}H)_2Os_3(CO)_{10}$ to give $(\mu\text{-}H)_2Os_3(CO)_{10}(L)$ complexes, which, when heated, produce $(\mu\text{-}H)_2Os_3(CO)_9(L)$ species.[4] One or both bridging hydrides can be replaced by bridging alkoxides[1] or thiolates.[5] Both the oxidative addition and the associative addition reactions involve donation of ligand electrons to $(\mu\text{-}H_2)Os_3(CO)_{10}$. In comparison to the parent carbonyl, the hydrido species loses two carbonyl ligands, representing four cluster electrons, and gains one H_2 unit, representing two cluster

(1) Johnson, B. F. G.; Lewis, J.; Kilty, P. *J. Chem. Soc. A* **1968**, 2859.
(2) (a) Deeming, A. J.; Hasso, S. *J. Organomet. Chem.* **1976**, *114*, 313. (b) Deeming, A. J.; Hasso, S. *Ibid.* **1975**, *88*, C21. (c) Keister, J. B.; Shapley, J. R. *J. Am. Chem. Soc.* **1976**, *98*, 1056. (d) Bryan, E. G.; Johnson, B. F. G.; Lewis, J. *J. Organomet. Chem.* **1976**, *122*, 249.
(3) (a) Deeming, A. J.; Hasso, S.; Underhill, M. *J. Organomet. Chem.* **1974**, *80*, C53. (b) Jackson, W. G.; Johnson, B. F. G.; Kelland, J. W.; Lewis, J.; Schorpp, K. T. *Ibid.* **1975**, *87*, C27.
(4) Deeming, A. J.; Hasso, S. *J. Organomet. Chem.* **1975**, *88*, C21.
(5) See, for example: Allen, V. F.; Mason, R.; Hitchcock, P. B. *J. Organomet. Chem.* **1977**, *140*, 297-307.

0020-1669/82/1321-3458$01.25/0

electrons. Therefore, there are two less electrons available for cluster bonding. This electron deficiency is responsible for the cluster's ability to act as a Lewis acid. However, $(\mu\text{-}H)_2Os_3(CO)_{10}$ can also be protonated.[6]

The structure of $(\mu\text{-}H)_2Os_3(CO)_{10}$ (**1**) is known from several

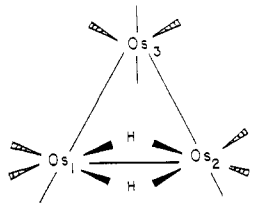

1

single-crystal diffraction studies.[7] Neither the Os–Os bond order nor any implications about the bonding are implied by the lines connecting atoms in **1**. The hydrogens are symmetrically disposed in a plane perpendicular to the plane containing the three Os atoms and are quite close to the Os_1–Os_2 edge. The Os_1–Os_2 bond distance is significantly shorter than either $Os_{1,2}$–Os_3 bond distance or the Os–Os bond distance in $Os_3(CO)_{12}$. The decrease in the Os_1–Os_2 distance can arise either from an increased metal–metal interaction or from the optimization of the Os–H interactions.

The question of the extent of direct metal–metal interaction between the Os_1 and Os_2 atoms remains unanswered. Earlier, several authors[2a,b,6] described the Os_1–Os_2 interaction as a true metal–metal double bond on the basis of the 18-electron rule. A simple symmetry treatment by Mason and Mingos[8a] emphasized the interaction of the bridging hydrogens with the metal d orbitals. The resultant occupied molecular orbitals are both metal–metal and metal–hydrogen bonding. Broach and Williams[7d] described a similar bonding scheme but emphasized the use of sp^3d^2 hybrids on the metal in forming the four-center, four-electron bond. Churchill, De Boer, and Rotella[8b] described the bond as a partially protonated double bond. Despite these various descriptions, the bonding in $(\mu\text{-}H)_2Os_3(CO)_{10}$ is still not well understood.

One can think of the formation of the complex as the protonation of metal–metal bonds of the dianionic precursor, **2**,

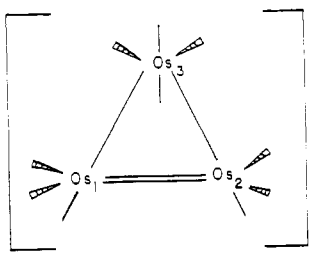

2

which contains a doubly bonded Os_1–Os_2 interaction to satisfy the 18-electron rule. In **2** each line is meant to represent a two-electron (2e) bond. An analogous process can be postulated for the electron-deficent main-group compound, diborane (B_2H_6), where the dianionic precursor, $B_2H_4^{2-}$, would have a boron–boron double bond. Although there is some direct boron–boron interaction in diborane,[9] the bonding is usually described as two three-center, two-electron (3c,2e) B–H–B bonds with no direct boron–boron bond. In the formation of diborane, the only electrons available for the protons to attack are those in the boron–boron double bond. Such is not the case in the attack of two protons on **2**, where, in addition to the electrons involved in the osmium–osmium double bond, each osmium has six "lone-pair" or pseudo-t_{2g} electrons, which are involved in the π bonding to the carbonyls. If the protons attacked these pseudo-t_{2g} electrons, the Os_1–Os_2 double bond could remain intact. Thus, for **2**, attack by protons could result in anything from two 3c, 2e Os–H–Os bonds with no direct Os_1–Os_2 bond, **3**, to two 3c, 2e Os–H–Os bonds with an Os_1–Os_2 double bond, **4**.

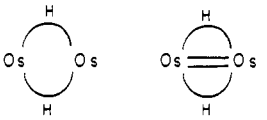

3 4

This study will examine the bonding in $(\mu\text{-}H)_2Os_3(CO)_{10}$ using ultraviolet photoelectron (PE) spectroscopy, a tool that has been successfully used to elucidate the electronic structure of many transition-metal complexes.[10] The spectrum will be interpreted both by comparison with the PE spectrum of the electron-precise $Os_3(CO)_{12}$ and by comparison with the results of parameter-free, Fenske–Hall molecule orbital (MO) calculations[11] on $Os_3(CO)_{12}$ and $(\mu\text{-}H)_2Os_3(CO)_{10}$. Using the PE spectrum and molecular orbital calculations, we will develop a consistent picture of the electronic structure and bonding in $(\mu\text{-}H)_2Os_3(CO)_{10}$. While this paper was being prepared, the spectrum of $(\mu\text{-}H)_2Os_3(CO)_{10}$ was reported by Green, Mingos, and Seddon,[10e] but it was not interpreted in detail nor were any MO calculations reported in this work.

Experimental and Theoretical Section

Preparation. The $(\mu\text{-}H)_2Os_3(CO)_{10}$ sample was kindly given to us by Professor Jack Lewis (Cambridge). Osmium carbonyl, $Os_3(CO)_{12}$, was purchased from Strem Chemical Co.

Spectroscopy. The ultraviolet photoelectron spectra were taken on a Perkin-Elmer Model PS-18 spectrometer. The total spectrum was recorded as a single slow scan, and the argon $^2P_{3/2}$ and $^2P_{1/2}$ lines at 15.76 and 15.94 eV were used as an internal reference. The resolution for all spectra was better then 30 meV for the fwhm of the Ar $^2P_{3/2}$ peak. No free CO spike at 14 eV was noted, indicating that both compounds were stable and did not decompose in the spectrometer.

Theory. Fenske–Hall MO calculations[11] were performed on an Amdahl 470 V/6 computer at Texas A&M University. Since no suitable Os functions are available, the actual calculations were done for $(\mu\text{-}H)_2Ru_3(CO)_{10}$ and $Ru_3(CO)_{12}$. The ruthenium basis functions were those of Richardson[12] et al. for Ru $4d^7$ and were augmented by 5s and 5p functions with exponents of 2.20. The carbon and oxygen functions were taken from the double-ζ basis set of Clementi.[13] An exponent of 1.20 was used for the hydrogen 1s function. Mulliken population analysis was used to determine the individual atomic charges and atomic orbital populations. Overlap populations between atoms were calculated and used to predict trends in the bond strength.

Since the covalent radii of Ru and Os are very close, the atomic positions for the Os and CO ligands were taken from the crystal

(6) Byran, E. G.; Jackson, W. G.; Johnson, B. F. G.; Kelland, J. W.; Lewis, J.; Schorpp, K. T. *J. Organomet. Chem.* **1976**, *108*, 385.
(7) (a) See ref 5. (b) Churchill, M. R.; Hollander, F. J.; Hutchison, T. P. *Inorg. Chem.* **1977**, *16*, 2260. (c) Orpen, G.; Rivera, A. V.; Bryan, E. G.; Pippard, D.; Sheldrick, G. M. *J. Chem. Soc., Chem. Commun.* **1978**, 723. (d) Broach, R. W.; Williams, J. W. *Inorg. Chem.*, **1979**, *18*, 314.
(8) (a) Mason, R.; Mingos, D. M. P. *J. Organomet. Chem.* **1973**, *50*, 53. (b) Churchill, M. R.; De Boer, B. G.; Rotella, F. J. *Inorg. Chem.* **1976**, *15*, 1843.
(9) Taylor, T. E.; Hall, M. B. *J. Am. Chem. Soc.* **1980**, *102*, 6136.
(10) (a) Turner, D. W.; Baker, C.; Baker, A. D.; Brundle, C. R. "Molecular Photoelectron Spectroscopy", 1st ed.; Wiley: New York, 1970. (b) Rabalais, J. W. "Principles of Ultraviolet Photoelectron Spectroscopy", 1st ed.; Wiley: New York, 1977. (c) Cowley, A. H. *Prog. Inorg. Chem.* **1980**, *26*, 45. (d) Chesky, P. T.; Hall, M. B. *Inorg. Chem.* **1981**, *20*, 4419 (part 1). (e) Green, J. C.; Mingos, D. M. P.; Seddon, E. A. *Inorg. Chem.* **1981**, *20*, 2595.
(11) Hall, M. B.; Fenske, R. F. *Inorg. Chem.* **1972**, *11*, 1619.
(12) Richardson, J. W.; Blackman, M. J.; Ranochak, J. E. *J. Chem. Phys.* **1973**, *58*, 3010.
(13) Clementi, E. *IBM J. Res. Dev.* **1965**, *9*, 2.

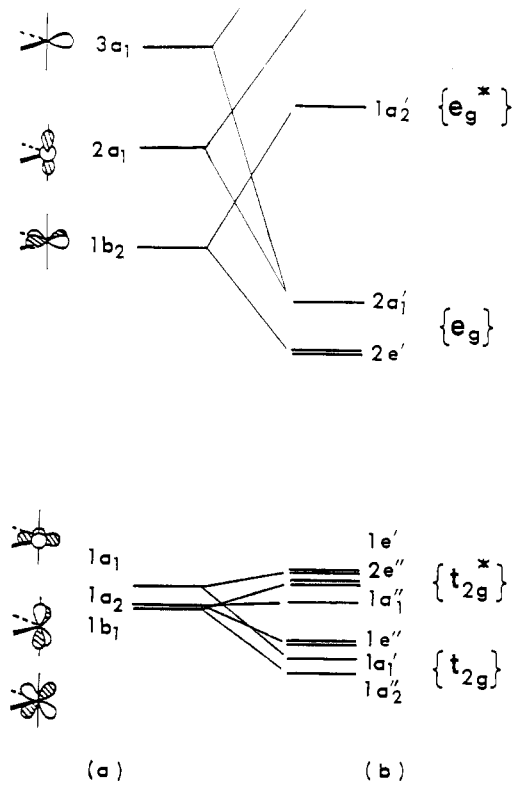

Figure 1. Molecular orbital diagram for the formation of $Os_3(CO)_{12}$ from three $Os(CO)_4$ fragments. The relative separation of the molecular orbitals is based on the results of Fenske–Hall molecular orbital calculations on the Ru analogue.

structure of Churchill et al.[7b] and were idealized for C_{2v} symmetry. The hydrogen atoms were placed at the positions determined in the neutron diffraction study of Orpen et al.[7c] The carbonyls were further idealized such that the two $Os(CO)_3$ fragments and the $Os(CO)_4$ fragment had C–Os–C angles of 90° and Os–C–O angles of 180°. Two calculations on $Os_3(CO)_{12}$ were performed: one with all Os–Os distances the same as the Os_1–Os_2 bond distance and another with all Os–Os distances the same as the $Os_{1,2}$–Os_3 bond distances of $(\mu\text{-H})_2Os_3(CO)_{10}$.

Results and Discussion

Ultraviolet Photoelectron Spectroscopy and Molecular Orbital Calculations of $Os_3(CO)_{12}$. Although the electronic structure of $Os_3(CO)_{12}$[14] and the photoelectron spectrum[10e,15] are well understood, a brief description of our results for this species is necessary to understand the results for $H_2Os_3(CO)_{10}$. Osmium carbonyl, **5**, can be viewed as a combination of three

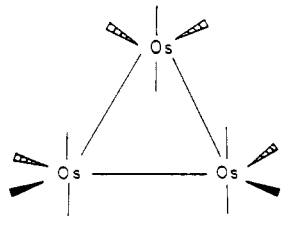

5

pseudooctahedral $Os(CO)_4$ fragments. The MO calculations on $Ru(CO)_4$ and $Ru_3(CO)_{12}$ were used to produce the molecular orbital diagram shown in Figure 1. Although this diagram is for the Ru analogues, we will use the diagram as a general diagram and will apply it to $Os_3(CO)_{12}$. The MO indexing begins with the first occupied orbital that is higher than the CO $5\sigma \rightarrow$ M d_σ bonds.

First, we consider the isolated $Os(CO)_4$ fragment (left side of Figure 1). The orbitals can roughly be grouped into three sets: a pseudo-t_{2g} set ($1b_1$, $1a_2$, $1a_1$) containing the three metal orbitals, which have lobes pointing off the Os–C internuclear axis and are stabilized by M $d_\pi \rightarrow$CO 2π back-donation, a pseudo-e_g set ($1b_2$, $2a_1$) containing the two metal orbitals, which have lobes pointing along the Os–C internuclear axis and are destabilized by CO $5\sigma \rightarrow$M d_σ donation, and a pseudo-a_{1g} orbital ($3a_1$), which contains mostly Os 6s and 6p character. The calculated splitting among the t_{2g} levels is small, they are all doubly occupied, and they are formally described as Os "lone-pair" orbitals. The t_{2g}–e_g splitting is large, a result consistent with the large crystal field splitting of the CO ligand and of the heavy metal. Within the pseudo-e_g set the $1b_2$ orbital is more stable than the $2a_1$ orbital because the $1b_2$ orbital is destablized by only two carbonyl donors whereas the $2a_1$ orbital is destabilized by four carbonyl donors. The pseudo-e_g orbitals contain a total of two electrons in the neutral $Os(CO)_4$ fragment. The $3a_1$ orbital is at higher energy because it is composed mainly of Os 6s and 6p atomic orbitals.

When three $Os(CO)_4$ fragments are brought together to form the united $Os_3(CO)_{12}$ molecule, there will be little mixing between the pseudo-t_{2g} orbitals and the pseudo-e_g orbitals because the t_{2g}–e_g splitting ($10Dq$) is large for $Os(CO)_4$. The pseudo-t_{2g} orbitals form a bonding set, $\{t_{2g}\}$, and an antibonding set, $\{t_{2g}^*\}$, with respect to metal–metal bonding. The MO calculations predict the ratio of orbitals, $\{t_{2g}\}/\{t_{2g}^*\}$, to be 4/5 with a small splitting between them. Since all of these pseudo-t_{2g} levels are doubly occupied, they contribute little to the metal–metal bonds.

The orbitals lying along the Os–Os internuclear axis are mainly derived from the pseudo-e_g orbitals of the $Os(CO)_4$ fragments. These form a bonding set, $\{e_g\}$, which is totally occupied and an antibonding set, $\{e_g^*\}$, which is unoccupied. The bonding $\{e_g\}$ transforms as doubly degenerate orbitals, which are combinations of the $Os(CO)_4$ fragment $1b_2$ orbitals, **6**, and as a singly degenerate orbital, which is a symmetric combination of fragment $2a_1$ orbitals and $3a_1$ orbitals, **7**. The

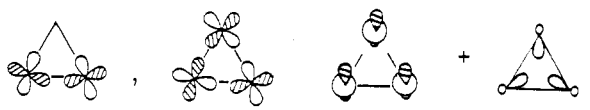

6 7

orbital shown in **7** is predicted to be the highest occupied molecular orbital (HOMO), preserving the $1b_2$–$2a_1$ splitting of the $Os(CO)_4$ fragment orbitals. The ratio of orbitals within $\{e_g\}$ is 1/2. the calculations predict that the splitting within $\{e_g\}$ is small compared to the $\{e_g\}$–$\{t_{2g}^*\}$ splitting.

With these results in mind it is relatively easy to interpret the PE spectrum of $Os_3(CO)_{12}$, Figure 2a. We have divided the band into three regions: I (7.8–9.0 eV), II (9.0–10.2 eV), and III (10.2–11.4 eV). The CO 5σ and 1π ionizations, which begin at 14 eV, are not shown. region III arises from ionizations of $\{t_{2g}\}$ and region II arises from ionizations of $\{t_{2g}^*\}$. Both broad bands have similar intensities, as predicted, and are separated by about 1.0 eV. The splitting between bands II and III is larger than the analogous bands in $Ru_3(CO)_{12}$, consistent with stronger metal–metal interactions. Region I corresponds to ionizations from $\{e_g\}$. The larger peak at higher ionization energy (IE) corresponds to the doubly degenerate $\{e_g\}$ orbitals and the small symmetric splitting is caused by Os spin–orbit coupling. The spin–orbit coupling of Ru is much smaller, and this feature is not observed in $Ru_3(CO)_{12}$.[10e,15]

(14) (a) Korol'kov, D. V.; Meissner, H. *Z. Phys. Chem. (Leipzig)* **1973**, *253*, 25. (b) Tyler, D. R.; Levenson, R. A.; Gray, H. B. *J. Am. Chem. Soc.* **1978**, *100*, 7888. (c) Schilling, B. E. R.; Hoffmann, R. *Ibid.* **1979**, *101*, 3456.

(15) (a) Green, J. C.; Seddon, E. A.; Mingos, D. M. P. *J. Chem. Soc., Chem. Commun.* **1979**, *94*. (b) Green, J. C.; Mingos, D. M. P.; Seddon, E. A. *J. Organomet. Chem.* **1980**, *185*, C20.

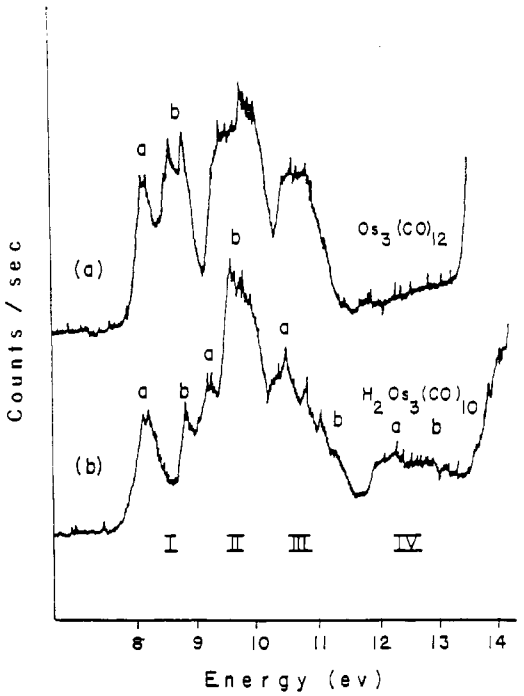

Figure 2. Photoelectron spectra of (a) $Os_3(CO)_{12}$ and (b) $(\mu\text{-}H)_2Os_3(CO)_{10}$.

The peak at the lowest IE (Ia) is the totally symmetric bonding combination of the $\{e_g\}$ set. The $\{e_g\}$ ionizations are well separated from the $\{t_{2g}^*\}$ and $\{t_{2g}\}$ ionizations, as predicted.

No attempt will be made to assign the features within the $\{t_{2g}\}$ or $\{t_{2g}^*\}$ sets of ionizations since the orbital energies are very closely spaced within each manifold. Our assignments of the PE spectrum of $(\mu\text{-}H)_2Os_3(CO)_{10}$ will be based on the general features described above.

Symmetry Considerations in the Bonding of $(\mu\text{-}H)_2Os_3(CO)_{10}$. Before examining the spectrum of $H_2Os_3(CO)_{10}$, we will briefly described what is well-known about the bonding from simple symmetry considerations, leaving the details of the MO calculations until later. The dihydrido species is composed of a pseudooctahedral $Os(CO)_4$ fragment, two pseudooctahedral $Os(CO)_3$ fragments, and an H_2 unit. The $Os(CO)_3$ fragment will have three pseudo-t_{2g} orbtials, which are fully occupied, and two pseudo-e_g orbitals, which have a total of two electrons.

Since the Os–Os bonds in $Os_3(CO)_{12}$ are formed primarily from the pseudo-e_g orbitals, it is reasonable to assume that the Os_1–Os_3 bond and the Os_2–Os_3 bond will be formed from this manifold. The H atoms, which are trans to the carbonyls of the $Os(CO)_3$ fragment, will also interact with the pseudo-e_g orbitals since they have lobes pointed directly at them. The four possible combinations of pseudo-e_g orbitals on Os_1 and Os_2 are shown in **8**–**11**, while Os_3 has the pseudo-e_g orbital

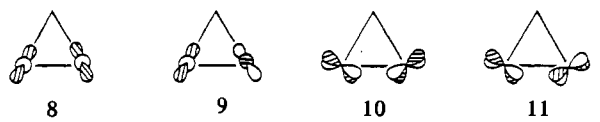

8 9 10 11

depicted in Figure 1. Clearly, the $Os_{1,2}$–Os_3 bonds must be like **12** and **13**. Thus, orbitals, **8** and **9** contribute nothing

12 13

to the Os_1–Os_2 bonding. Of the remaining pseudo-e_g bonding orbitals, **10** and **11**, only **10** will interact strongly with the H ligands would be an Os_1–Os_2 π-bonding orbital in a system

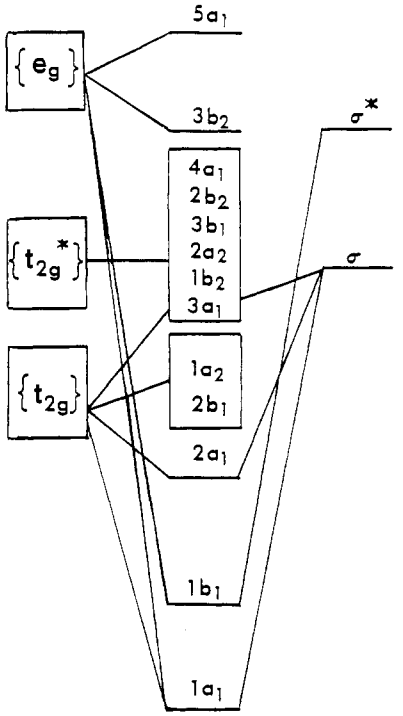

Figure 3. Molecular orbital diagram for $(\mu\text{-}H)_2Os_3(CO)_{10}$ compared to those of $Os_3(CO)_{12}$ and H_2. The relative energies of $Os_3(CO)_{12}$ and $(\mu\text{-}H)_2Os_3(CO)_{10}$ are based on the photoelectron spectra.

like $Os_3(CO)_{10}^{2-}$, will be less Os–Os bonding and more Os–H bonding. In addition to interacting with the pseudo-e_g orbitals, the H atoms also interact with the pseudo-t_{2g} orbitals. The question of direct Os_1–Os_2 bonding in $(\mu\text{-}H)_2Os_3(CO)_{10}$, therefore, will involve considerations of orbitals beyond those considered in the bonding of $Os_3(CO)_{12}$. The double hydrido bridge makes possible a complicated and unique system of metal–metal bonding, which will be discussed in detail after examining the PE spectrum of $(\mu\text{-}H)_2Os_3(CO)_{10}$.

Photoelectron Spectrum of $(\mu\text{-}H)_2Os_3(CO)_{10}$. The PE spectrum of dihydridotrisomium decacarbonyl is shown in Figure 2b. The new bands appearing in region IV (11.4–13.6 eV) are due to ionization from metal–hydrogen bonding orbitals. This is consistent with the PE spectra of other transition-metal complexes with bridging hydrogens.[10e,15,16] The bands correspond to the symmetric and antisymmetric combinations of H atomic orbitals but are not well resolved. Part of region III, which can be assigned to the $\{t_{2g}\}$ ionizations like region III of $Os_3(CO)_{12}$, has been stabilized and appears at higher ionization energy. Region II can be roughly assigned as the $\{t_{2g}^*\}$ ionizations as in the spectrum of $Os_3(CO)_{12}$. The peak centered at 9.6 eV (IIb) has gained intensity relative to the other metal peaks in the spectrum, while intensity has been lost from the leading edge of region II compared to region II of $Os_3(CO)_{12}$. Region I, which contained the metal–metal bonds, $\{e_g\}$, in $Os_3(CO)_{12}$, has lost intensity and appears to consist of only two ionizations. The change in region I is consistent with a loss of the Os_1–Os_2 $\{e_g\}$ bonding, as this orbital is now being used for Os–H bonding. The two peaks correspond to the two remaining $Os_{1,2}$–Os_3 bonding orbitals discussed in the previous section (**12**, **13**).

The spectrum of $(\mu\text{-}H)_2Os_3(CO)_{10}$ can be more quantitatively interpreted by comparison with the MO calculations. An *experimental* MO diagram for $Os_3(CO)_{12}$ and $(\mu\text{-}H)_2Os_3(CO)_{10}$ is shown in Figure 3. The $Os_3(CO)_{12}$ energy levels, Figure 3, are plotted at the IEs of the bands in the

(16) (a) Wong, K. S.; Dutta, T. K.; Fehlner, T. P. *J. Organomet. Chem.* **1981**, *215*, C48. (b) Sherwood, D. E., Jr.; Hall, M. B., submitted for publication in *Organometallics*.

parent carbonyl. Although $(\mu\text{-H})_2Os_3(CO)_{10}$ is made from different pseudooctahedral fragments, it will have the same number of bonding and antibonding combinations of pseudo-e_g and pseudo-t_{2g} orbitals. Therefore, $Os_3(CO)_{12}$ metal levels can be used as a starting point for discussing the interactions in the dihydrido species.

There are two ways in which the two hydrogen bridges can affect the position of the metal bands in the PE spectrum: either by direct interaction with the formation of bonding and antibonding orbitals or by indirect charge stabilization of the metal orbitals. Charge stabilization occurs if the hydrogen atoms withdraw electrons from the Os atoms, i.e., if they have some hydridic character. Atomic charges of the hydrogens in $(\mu\text{-H})_2Os_3(CO)_{10}$ were calculated to be 0.351−. The Os_1 and Os_2 atoms have a charge of 0.336+, whereas the Os atom with four CO ligands (Os_3) has a charge of 0.185−. This charge difference causes a lowering of the Os 5d orbital energy for Os_1 and Os_2 relative to that of Os_3. The hydrogens then interact with these low-energy orbitals, which are rich in Os_1 and Os_2 metal d character.

The molecular orbital diagram for $(\mu\text{-H})_2Os_3(CO)_{10}$ has the energies plotted at the position Os_1–H–Os_2 the ionization potentials found in the PE spectrum while the assignments are based on MO calculations. It is easier to examine the interaction of the two H atoms with of cluster if we first form the symmetric and antisymmetric linear combinations of the H orbitals, H_2 σ and H_2 σ^*. The H_2 σ orbital interacts strongly with two of the $\{t_{2g}\}$ orbitals, forming the $1a_1$, $2a_1$, and $3a_1$ orbitals **14**, **15**, and **16**, respectively, which are bonding,

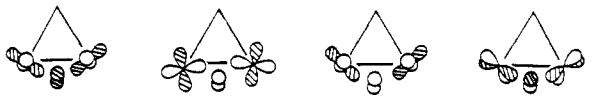

14 15 16 17

nonbonding, and antibonding combinations. The $1a_1$ orbital is stabilized further by interactions with the $\{e_g\}$ orbital, **8**. The symmetric $1a_1$ orbital is responsible for peak IVb, Figure 2b. The H_2 σ^* orbital interacts strongly with the other Os_1–Os_2 $\{e_g\}$ bonding orbital, **10**, forming the $1b_1$, **17**, which is responsible for peak IVa, Figure 2b.

The $2a_1$ orbital, which is primarily $\{t_{2g}\}$, is stabilized by both Os_1–Os_2 and Os_1–H–Os_2 bonding interactions and appears as the shoulder, IIIb in Figure 2b. The $3a_1$ orbital, while metal–metal bonding, is destabilized by the metal–hydrogen antibonding interaction and is pushed to lower IE. While the position of this band cannot be absolutely assigned, the calculations indicate that it is pushed up into the $\{t_{2g}^*\}$ region adding intensity to region IIb. The $1a_2$ and $2b_1$ orbitals remain $\{t_{2g}\}$ orbitals, which are relatively unaffected by the H's, and appear as the broad band, IIIa, in Figure 2b. They are composed primarily of bonding combination of the pseudo-t_{2g} orbitals of Os_1 and Os_2, which have poor overlap with H orbitals, with contributions from the pseudo-t_{2g} orbitals of the $Os(CO)_4$ fragment.

The $\{t_{2g}^*\}$ orbital energies are closely spaced, and no attempt will be made to assign individual peaks. The calculations indicate that the three highest energy orbitals (least stable) in the $\{t_{2g}^*\}$ set are localized on the $Os(CO)_4$ fragment but contain significant Os_1 and Os_2 character. Intensity has shifted from the leading edge (band IIa) to the trailing edge (band IIb) in $(\mu\text{-H})_2Os_3(CO)_{10}$ relative to region II in $Os_3(CO)_{12}$. This is consistent with the indirect charge stabilization of the 5d orbitals of Os_1 and Os_2 by the H ligands as predicted by the MO calculation. The $\{t_{2g}^*\}$ orbitals with localized $Os(CO)_4$ character will be split by spin–orbit coupling, and one component, peak IIa, is pushed to a lower IE than the $\{t_{2g}^*\}$ of $Os_3(CO)_{12}$. The calculations indicate that peaks Ia and Ib correspond to the orbitals **12** and **13**, respectively.

Table I. Metal–Metal Overlap Populations

bond	overlap populations			
	total	d–d	e_g–e_g	t_{2g}–t_{2g}
$Os_{1,2}$–Os_3	0.131	0.017	0.020	−0.005
Os_1–Os_2	0.089	0.017	0.004	0.011

Bonding in $(\mu\text{-H})_2O_3(CO)_{10}$. The molecular orbital calculations can be used to describe additional details of the electronic structure and bonding in $(\mu\text{-H})_2Os_3(CO)_{10}$. The metal–hydrogen bonding occurs with the pseudo-e_g, 6s, and 6p orbitals of the $Os(CO)_3$ fragments. While the H orbitals do interact strongly with the $\{t_{2g}\}$ set, which is composed primarily of bonding combinations of $Os(CO)_3$ pseudo-t_{2g} atomic orbitals, both the bonding and antibonding orbitals are filled, leaving no net osmium–hydrogen bond with the $\{t_{2g}\}$ orbitals.

As suggested by the overlap populations in Table I, the metal–metal interactions are more complicated. The total metal–metal overlap population for the Os_1–Os_2 interaction is somewhat smaller than that for the $Os_{1,2}$–Os_3 interactions. Although their d–d overlap populations are equal, the distribution of the direct d–d bonding is considerably different. For the $Os_{1,2}$–Os_3 bonds the net d bonding occurs primarily between the e_g-type orbitals, but for the Os_1–Os_2 bond it is the t_{2g}-type orbitals that contribute the most to the overlap population. This reversal of roles is an important feature of the dihydrido-bridged interaction. The dihydrogen bridge increases the t_{2g}–t_{2g} bonding but destroys the e_g–e_g bonding.

For a better understanding of the Os_1–H–Os_2 interactions, the revalent molecular orbitals were plotted in a plane midway between Os_1–Os_2 and H–H and perpendicular to the $Os_{1,2}$–Os_3 plane. The three H $\{t_{2g}\}$ bonding orbitals, $1a_1$, $2a_1$, and $3a_1$, are shown in Figure 4, parts a, b, and c, respectively. Solid and dashed contours represent positive and negative signs of the wave function. All three orbitals clearly show metal–metal bonding interactions. The $1a_1$ orbital is both Os–Os and Os–H bonding. $2a_1$ contains both bonding and antibonding Os–H interactions, and the contours crossed in the Os–H direction are fewer than in the Os–Os direction, indicating that this orbital is more Os–Os than Os–H bonding. The $3a_1$ orbital is Os–Os bonding but is antibonding with the H_2 σ-bonding orbital, which is perpendicular to the Os_1–Os_2 internuclear axis. The $1a_1$ and $3a_1$ orbitals cancel most of the H to $\{t_{2g}\}$ bonding. The $2a_1$ is stabilized mainly by direct Os_1–Os_2 interactions. The $1a_1$ and $2a_1$, particularly, are sufficiently stabilized that their CO 2π character is reduced and their Os character is increased. It is this feature that allows net t_{2g}-type bonding when two Os atoms are doubly bridged by hydrogen atoms.

The $1b_1$ orbital, the H to $\{e_g\}$ bonding orbital (Figure 4d), is more Os–H than Os–Os bonding as the highest valued contours occur around the hydrogen atom. This orbital accounts for 74% of the Os 5d–H 1s overlap population and 30% of the Os_1 5d–Os_2 5d overlap population. The two highest occupied molecular orbitals are the $Os_{1,2}$–Os_3 bonds, $3b_2$ and $5a_1$ (Figure 4e,f). These orbitals are Os_1–Os_2 antibonding and bonding, respectively, and they contribute little to the net Os_1–Os_2 bond. The HOMO, $5a_1$, contains significant Os–H antibonding character and appears at a higher energy than the $3b_2$ orbital.

This molecule also possesses a low-lying unoccupied molecular orbital, the $3a_2$ orbital (Figure 4g). This orbital is antibonding with respect to the Os_1 and Os_2 atoms. It will interact strongly with donor ligands that have filled p orbitals, which are antisymmetric with respect to the Os_1–Os_2 interaction. This partially explains the increase in Os_1–Os_2 bond lengths found for complexes where the hydrido hydrogens are successively replaced by bridging methoxide ligands. The Os_1–Os_2 bond distance lengthens on going from $(\mu\text{-H})_2Os_3$-

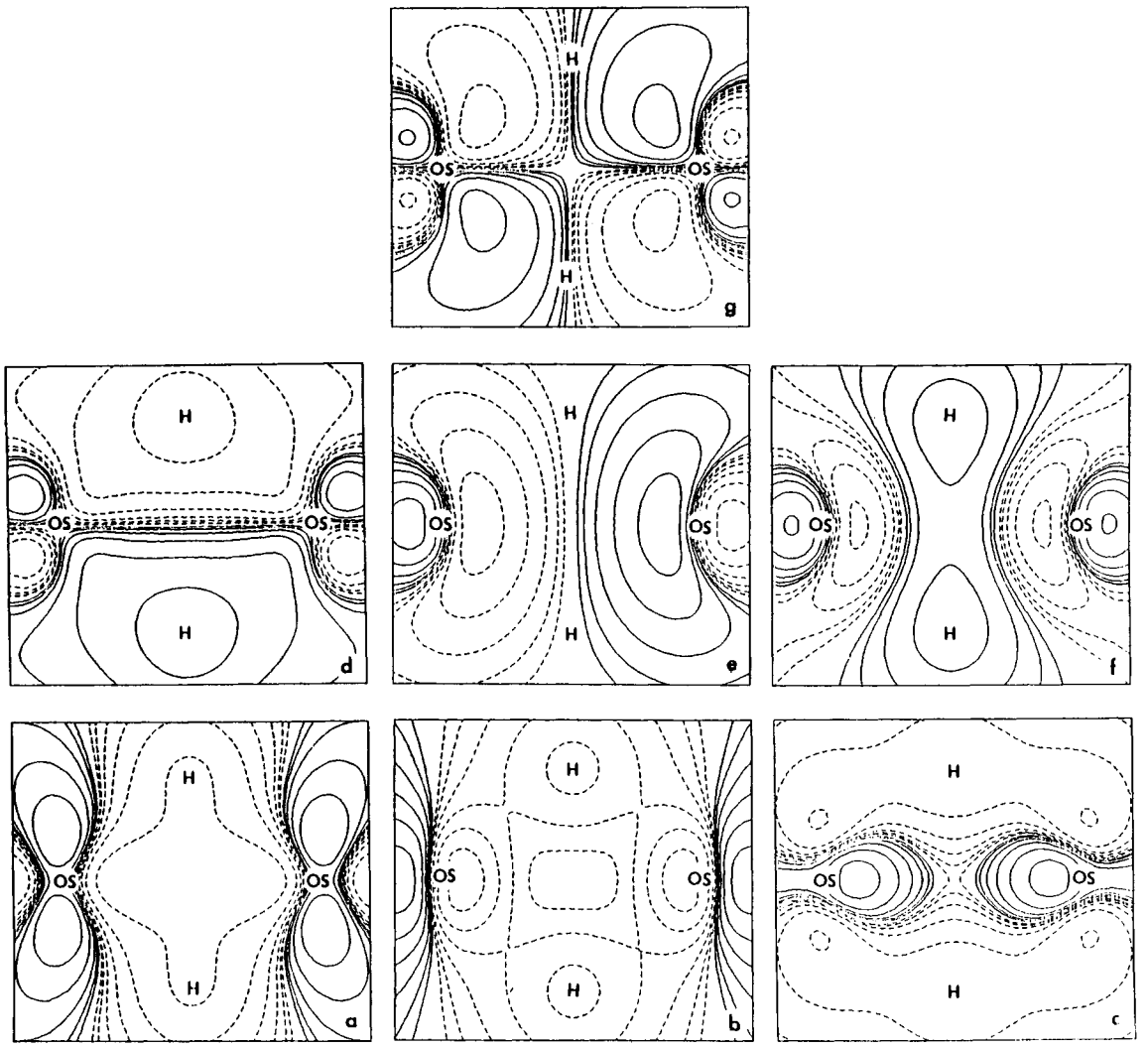

Figure 4. Plots of the molecular orbitals with significant $Os_{1,2}$-H character in a plane between the Os_1–Os_2 and H–H bonds. The pseudo-t_{2g} interactions, $1a_1$, $2a_1$, and $3a_1$, are shown in parts a, b, and c, respectively. The pseudo-e_g, $1b_1$, is shown in part d. The $Os_{1,2}$–Os_3 bonds, $3b_2$ and $5a_1$, are shown in parts e and f, respectively. The lowest unoccupied orbital, $3a_2$, is shown in part g.

$(CO)_{10}$ ($R_{Os_1-Os_2}$ = 2.670 Å) to $(\mu\text{-H})(\mu\text{-OMe})Os_3(CO)_{10}$ ($R_{Os_1-Os_2}$ = 2.863 Å) to $(\mu\text{-OMe})_2Os_3(CO)_{10}$ ($R_{Os_1-Os_2}$ = 3.078 Å). Previous authors have interpreted this as going from a double bond to a single bond to no bond for Os_1–Os_2. Each step does not involve addition of two extra electrons to some virtual metal–metal antibonding orbital in $(\mu\text{-H})_2Os_3(CO)_{10}$ as was postulated by Mason and Mingos.[8a] The changes in bond distance are too small for this interpretation. The methoxide ion, H_3CO^-, possesses an oxygen atom with three lone pairs of electrons. One lone pair will form a bond with the same metal orbitals as the hydridic hydrogens do in $(\mu\text{-H})_2Os_3(CO)_{10}$. The other two O lone-pair orbitals form a symmetric and an antisymmetric combination with respect to the Os_1–Os_2 interaction; both will be doubly occupied in the molecule. The effect of the antisymmetric donor orbital is twofold. First, it will be stabilized by mixing with $3a_2$ orbital, which will cancel to some extent the Os_1–Os_2 pseudo-e_g bonding in the $1b_1$ osmium–hydrogen bonding orbital. Second, this interaction involves oxygen to osmium charge transfer. The symmetric donor orbital will interact with the pseudo-t_{2g}, again with the O→Os electron donation. This will disrupt the pseudo-t_{2g} stabilization by charge destabilization. With two methoxide ligands, the $\{t_{2g}\}$ and $\{t_{2g}^*\}$ orbitals will be more like those of $Os_3(CO)_{12}$, which are essentially nonbonding.

Conclusions

Unlike the case of diborane, the bridged Os–Os distance in $(\mu\text{-H})_2Os_3(CO)_{10}$ is actually shorter than an unsupported single-bond distance. Although the major part of the bonding in the $(\mu\text{-H})_2Os_2$ system is composed of two three-center, two-electron Os–H–Os bonds, as in diborane, there is an additional bonding interaction in the $(\mu\text{-H})_2Os_2$ bridge not present in diborane. Our calculations and the PE spectrum suggest that the $(\mu\text{-H})_2$ bridge causes stabilization of the in-phase (bonding) combinations of the pseudo-t_{2g} orbitals. Net "t_{2g}–t_{2g}" bonding results because the carbonyls preferentially back-bond to the less stable, out-of-phase (antibonding) combinations of the pseudo-t_{2g} orbitals. We believe it is this additonal bonding interaction, not available in diborane, that is responsible for the short M–M distance in $(\mu\text{-H})_2M_2$ systems such as $H_2Os_3(CO)_{10}$,[7] $H_2Re(CO)_8$,[17] and $H_2W_2(CO)_8^{2-}$.[18]

Usually these pseudo-t_{2g} electrons are thought not to participate in M–M bonding of clusters.[14c,19] However, there is a distinct possibility that these pseudo-t_{2g} electrons are involved in the bonding of simple binary carbonyl clusters. With He II radiation, PE spectra of a number of clusters[10e,15] show an increase in the intensity of the bonding $\{t_{2g}\}$ band compared to the antibonding $\{t_{2g}^*\}$ band. If the larger metal character in $\{t_{2g}\}$ implied by this intensity change is due to differential CO back-bonding, net "t_{2g}–t_{2g}" bonding could result. Further

(17) Bennett, M. J.; Graham, W. A. G.; Hoyano, J. K.; Hucheon, W. L. *J. Am. Chem. Soc.* **1972**, *94*, 6232.
(18) Churchill, M. R.; Chang, S. W. *Inorg. Chem.* **1974**, *13*, 2413.
(19) Hoffmann, R. *Science* **1981**, *211*, 995.

work is needed to prove or disprove this hypothesis for the binary carbonyl clusters.

Acknowledgment is made to the Robert A. Welch Foundation (Grant A-648) and the National Science Foundation (Grant CHE 79-20993) for their support.

Registry No. $(\mu\text{-H})_2Os_3(CO)_{10}$, 41766-80-7.

Supplementary Material Available: A listing of percent character of molecular orbitals (10 pages). Ordering information is given on any current masthead page.

Contribution from the Department of Chemistry, The University of New England, Armidale, NSW Australia, 2351

Average and Single-Crystal Magnetic Properties of Potassium Bis(carbonato)cuprate(II): A Three-Dimensional Ferromagnet

ANTHONY K. GREGSON* and NEVILLE T. MOXON

Received March 10, 1982

Average and single-crystal magnetic measurements on the three-dimensional potassium bis(carbonato)cuprate(II) show that this material orders ferromagnetically at 6.6 K. Above 15 K the data are well represented by the $S = {}^1/_2$ series expansion for the three-dimensional fccub lattice with $g = 2.14$ and $J = 1.19$ cm^{-1}. $K_2Cu(CO_3)_2$ appears to be the best example of a three-dimensional $S = {}^1/_2$ Heisenberg ferromagnet yet studied.

Introduction

Many different compounds can be isolated from aqueous solutions containing copper(II) and carbonate ions, depending on the conditions and the other cations present. For example, $Na_2Cu(CO_3)_2 \cdot 3H_2O$ has a discrete chainlike structure,[1-3] and $Cu(NH_3)_2CO_3$ possesses a complicated intertwinned structure[4] whereas $Na_2Cu(CO_3)_2$ has a two-dimensional network of $[Cu(CO_3)_2^{2-}]_\infty$, successive layers being bound by the sodium ions.[5] We have reported recently the magnetic properties of each of these materials. Susceptibility measurements on $Na_2Cu(CO_3)_2 \cdot 3H_2O$ provide evidence for ferromagnetic intrachain interactions.[6] We have also reanalyzed the magnetic susceptibility data on $Cu(NH_3)_2CO_3$ using a cluster approximation.[7] This material has an approximately two-dimensional structure with two different in-plane metal–metal interactions which are both antiferromagnetic in nature. Average[8] and single-crystal[9] magnetic measurements on $Na_2Cu(CO_3)_2$ show that this compound possesses ferromagnetic intralayer exchange interactions although it orders antiferromagnetically at 5.6 K. Spin–flop behavior was observed below 5.6 K.

We have also prepared and determined the crystal structure of another member of this system, namely, $K_2Cu(CO_3)_2$.[10] The basic crystallographic data are summarized in the Experimental Section. The structure is, suprisingly, somewhat different from $Na_2Cu(CO_3)_2$; the symmetry is higher, and although the structure comprises planar CuO_4 chomophores linked by bridging bidentate carbonate groups, with embedded potassium cations, it is more subtle and three dimensional in nature (Figure 1). The four oxygen atoms about each copper atom form a plane roughly parallel to the *ab* plane of the crystal. To this extent the structure is very similar to that of the sodium derivative. However, in the potassium derivative each bidentate carbonate group is oriented such that it coordinates to copper atoms 0.25 apart in *z*. Rather than propogating a planar structure, this has the effect of making a three-dimensional polymeric network of copper atoms connected by the bidentate carbonate groups. This subtle change in structure gives rise to different magnetic properties, which are reported herein.

Experimental Section

The preparation of $Na_2Cu(CO_3)_2$ proceeds via $Na_2Cu(CO_3)_2 \cdot 3H_2O$.[1,8,9] However, in the preparation of the potassium derivative we were unable to isolate the trihydrate so we proceeded directly with the preparation of anhydrous $K_2Cu(CO_3)_2$.[10] A nearly saturated solution of K_2CO_3 [K_2CO_3 (150 g) in boiling water (110 cm^3)] was cooled to slightly below 50 °C, and copper acetate monohydrate (20 g) was added with stirring. It is important that the temperature does not go above 50 °C because CuO will begin to form. The resulting solution was deep purplish blue, but on standing overnight, it turned into a thick pale blue gelatinous precipitate, which was difficult to characterize. Presumably this contains a hydrated form of $K_2Cu(CO_3)_2$. However, when the solution was allowed to stand for a week or more small, well-formed, very dark blue platelike crystals of anhydrous $K_2Cu(CO_3)_2$ formed, which were suitable for both crystallographic and magnetic work. The crystal structure of $K_2Cu(CO_3)_2$ has been determined[10] by single-crystal X-ray diffraction at 295 (1) K and refined by full-matrix least squares to a residual of 0.027 for 1441 "observed" reflections. Crystals are orthorhombic, of space group *Fdd*2, with $a = 11.425$ (3) Å, $b = 17.658$ (4) Å, $c = 6.154$ (2) Å, and $Z = 8$. The structure comprises potassium cations embedded in an infinite three-dimensional polymeric anionic array of square-planar coordinated copper atoms with bridging carbonate groups [Cu–O = 1.934 (2), 1.936 (2) Å]. Within the latter, the noncoordinating oxygen–carbon bond is shorter [1.259 (3) Å] than the other two [1.303 (3), 1.307 (2) Å] and the O–C–O angle opposite it is

(1) Brotherton, P. D.; White, A. H. *J. Chem. Soc., Dalton Trans.* **1973**, 2338.
(2) Harlow, R. L.; Simonsen, S. H. *Acta Crystallogr., Sect. B* **1975**, *B31*, 1313.
(3) Mosset, A.; Bonnet, J. J.; Galy, J. *Z. Kristallogr.* **1978**, *148*, 165.
(4) Meyer, M. H.; Singh, P.; Hatifield, W. E.; Hodgson, D. J. *Acta Crystallogr., Sect. B* **1972**, *B28*, 1607.
(5) Healy, P. C.; White, A. H. *J. Chem. Soc., Dalton Trans.* **1972**, 1913.
(6) Gregson, A. K.; Moxon, N. T.; Weller, R. R.; Hatfield, W. E. *Aust. J. Chem.*, in press.
(7) Gregson, A. K.; Weller, R. R.; Hatfield, W. E. *Inorg. Chem.* **1980**, *19*, 3436.
(8) Gregson, A. K.; Healy, P. C. *Inorg. Chem.* **1978**, *17*, 2969.
(9) Gregson, A. K.; Moxon, N. T. *Inorg. Chem.* **1981**, *20*, 78.
(10) Farrand, A.; Gregson, A. K.; Skelton, B. W.; White, A. H. *Aust. J. Chem.* **1980**, *33*, 431.

0020-1669/82/1321-3464$01.25/0